A Deterministic Compressed GNSS Acquisition Technique

Seung-Hyun Kong, *Member, IEEE*

***Abstract*—In the cold start of a Global Navigation Satellite Systems (GNSS) receiver, fast acquisition of the GNSS signal requires either an extensive usage of hardware resources for massive parallel correlators or a high computational complexity for fast Fourier transform (FFT) and inverse FFT operations. Because GNSS uses direct-sequence spread spectrum (DSSS) signaling with binary phase-shift keying (BPSK) or with BPSK and binary offset carrier, any GNSS signal can have a sparse representation so that the concept of compressed sensing can be applied to detect GNSS signals. To achieve a fast acquisition of the GNSS signal with a reduced number of correlators and low computational complexity, we propose a two-stage deterministic compressed GNSS acquisition technique using the Walsh–Hadamard matrix. The proposed technique makes fast acquisition possible for a receiver using a much smaller number of correlators than the conventional parallel-correlator-based technique, which requires much less computational complexity than the FFT-based technique. We provide complexity analysis of the proposed technique and compare the statistical performance of the proposed technique with other techniques applicable to the fast GNSS acquisition. The proposed technique is easy to implement and is the first compressed-sensing-based GNSS acquisition technique.**

***Index Terms*—Compressed sensing (CS), direct spread spectrum, Global Navigation Satellite System (GNSS), signal acquisition.**

I. Introduction

In a cold start, the first task for a Global Navigation Satellite System (GNSS) receiver is to execute signal acquisition, which is mostly signal search by testing all likely 2-D hypotheses of the code phase and the Doppler frequency of the incoming GNSS signal [1]. For a fast completion of the signal acquisition task, a conventional receiver is generally equipped with massive parallel correlators. In general, it takes a longer acquisition time to test a large number of hypotheses with fewer correlators. Therefore, reducing both the number of correlators and the acquisition time in a cold start is not an easy task for a conventional GNSS receiver. An alternative, i.e., the fast Fourier transform (FFT)-based GNSS signal acquisition technique using a digital signal processor for fast computation, has gained much attention because it can quickly complete the hypothesis-testing process without requiring a large amount of hardware resources, i.e., massive correlators. In general, the FFT-based technique requires FFTs of the incoming signal and the receiver's code replica, complex multiplications in the frequency domain, and an inverse fast Fourier transform (IFFT) of the frequency-domain signal [2]. To summarize, an ideal GNSS signal acquisition technique may be the one that can quickly complete the acquisition task while using a lower number of correlators and lower computational power in the receiver than other conventional parallel-correlator- and FFT-based techniques, respectively.

Folding techniques [3], [4] are some of the recent technologies used for fast GNSS acquisition. In folding techniques, the receiver's code replica is folded, and correlation is performed between the folded signal and incoming signal. The folding technique is similar to the conventional parallel-correlator-based technique in the sense that multiple code-phase hypotheses are simultaneously tested, but the technique suffers from signal-to-noise ratio (SNR) degradation as the number of folding increases.

Another recent technique that can achieve fast GNSS acquisition may be deterministic compressed sensing (CS). In general, CS exploits the sparsity of a signal to reduce the number of measurements required for successful representation of the signal. Theoretically, the CS technique finds the solution of a classical underdetermined system of linear equations [5]–[7]; it reconstructs an arbitrary K-sparse (i.e., K nonzeros and $N-K$ zeros) signal $\mathbf{x}_K$ of size $[N \times 1]$ from a set of $M (K < M < N)$ linear measurements $\mathbf{y}$ (i.e., size $[M \times 1]$) obtained using a measurement matrix $\mathbf{\Phi}$ of size $[M \times N]$ such that $\mathbf{y} = \mathbf{\Phi x}_K$. Note that the size of $\mathbf{y}$ should be at least N to perfectly reconstruct $\mathbf{x}_K$ in a conventional system of linear equations and that $\mathbf{x}_K$ carries only K number of information. The technique is also useful to practical cases such as when $\mathbf{x}_K$ is approximately sparse (i.e., $\mathbf{x}_K$ is mostly noisy nonzeros but has only K dominant elements, which are the most of the information contained within $\mathbf{x}_K$), and the reconstruction process is to find K dominant elements of $\mathbf{x}_K$ from $\mathbf{y}$. Because GNSS uses direct-sequence spread spectrum (DSSS), an incoming GNSS signal can be well expressed with a very small amount of information, its code phase, and Doppler frequency, provided that the spreading sequence is known to the receiver. Therefore, when the GNSS-receiver-generated Doppler frequency is close to the incoming GNSS signal, for example, a GPS coarse/acquisition

Manuscript received April 30, 2012; revised August 3, 2012; accepted September 21, 2012. Date of publication September 28, 2012; date of current version February 12, 2013. This work was supported by the National Research Foundation of Korea through the Korean Ministry of Education, Science, and Technology under Grant 2011-0025867. The review of this paper was coordinated by Prof. X. Wang.

The author is with the CCS Graduate School for Green Transportation, Korea Advanced Institute of Science and Technology, Daejeon 305-701, Korea (e-mail: skong@kaist.ac.kr).

Color versions of one or more of the figures in this paper are available online at http://ieeexplore.ieee.org.

Digital Object Identifier 10.1109/TVT.2012.2220989

(C/A) code has $N = 1023$, but K can be as small as 1 if the signal is represented in the correlation domain, where the signal becomes the sparsest. As a result, the number of correlators to detect the incoming GNSS signal can be much smaller than N, whereas for the conventional GNSS acquisition technique, a receiver needs to make N measurements to test N code-phase hypotheses. Therefore, the acquisition of a GNSS signal can exploit the concept of CS to reduce the required number of measurements yielded by correlators. For a successful application of the CS, it is necessary to find an appropriate transformation (sparsifying) matrix to most sparsely express the target signal and to develop a measurement matrix along with an associated efficient reconstruction algorithm. So far, a number of measurement matrices and successful reconstruction algorithms have been introduced. For example, random Gaussian and random Bernoulli matrices are known as general measurement matrices in random CS, but the associated reconstruction algorithms have high computational complexity [5]–[7]. On the other hand, CS techniques using deterministic measurement matrices have much lower computational complexity for reconstruction. The Vandermonde matrix [8], chirp matrix [9], and the matrix with columns of second-order Reed–Muller (RM) code [10], [11] (a binary equivalent matrix to the chirp matrix) are some examples of measurement matrices in deterministic CS that can achieve fast reconstruction of the signal. However, the deterministic CS matrices are not very robust to noisy input signal, i.e., signal of low SNR.

The GNSS signal can have a very sparse expression in the autocorrelation output, where the signal can be expressed with only one dominant peak when the SNR is good enough. However, because the spreading sequence used in GNSS is the Gold code and the autocorrelation of the Gold code is noisy [1], applying deterministic CS techniques [8]–[10] to the GNSS acquisition may not produce a successful result when the SNR is not high enough. In this paper, we propose a two-stage fast GNSS signal acquisition technique using GNSS specific deterministic CS matrices to reduce both the computational complexity and hardware consumption while achieving higher noise robustness than the folding techniques and other deterministic CS matrices. It is shown that algebraic expressions for the performance of the simplest implementation of the proposed technique are identically the same to those of the parallel-correlator-based acquisition technique, with a modification to the SNR of the incoming signal and the number of parallel correlators.

The rest of this paper is organized as follows. In Section II, the first-stage measurement matrix is introduced. In Section III, the second-stage measurement matrix is introduced, and the decoding algorithms for the first- and the second-stage measurement output are described. Section IV shows the mathematical analysis of the performance of the proposed technique, and Section V discusses a comparison of the proposed technique to other techniques. To demonstrate the performance of the proposed technique, Monte Carlo simulations in additive white Gaussian noise (AWGN) channels and Rayleigh fading channels, and field tests are carried out to compare with the conventional parallel-correlator-based technique in Section VI, and conclusions are drawn in Section VII.

II. Compressed Measurement in the First Stage

Let $r(t)$ represents an incoming GNSS signal to a receiver, i.e.,

$$r(t) = A^s D^s(t-\tau^s) P^s(t-\tau^s) e^{j(2\pi(f_{L1}+f_D^s)t+\theta^s)} + n(t) \quad (1)$$

where A^s, τ^s, f_{L1}, f_D^s, and θ^s are the amplitude, code phase, carrier frequency, Doppler frequency, and unknown carrier phase of the received signal, respectively. $D(t)^s$, $P(t)^s$, and $n(t)$ represent navigation data at R_b bps, GNSS spreading code at R_c chips per second (cps; $R_c = (1/T_c) \gg R_b$), and a complex AWGN process with two-sided power spectral density $(N_0/2)$, respectively [1], and $(\cdot)^s$ denotes the sth satellite. A GNSS signal acquisition process finds the code-phase delay τ and the Doppler frequency f_D^s of the incoming signal, which becomes a 2-D search process. Because the receiver needs to find the code phase of the incoming signal within a half-chip $(T_c/2)$ accuracy, the sampling rate $f_s = (1/T_s)$ that we assume is two times the chip rate of the spreading code $f_s = 2R_c$, which follows the Nyquist sampling theorem and is a general choice in GNSS acquisition systems. In the 2-D search, the receiver multiplies the received signal $r(t)$ (1) by $e^{-j2\pi(f_{L1}+f_F)t}$ to remove the carrier frequency, where f_F is the current Doppler frequency hypothesis made by the receiver such that

$$f_F = f_{D,\min}^s + F\Delta f \quad (2)$$

where $f_{D,\min}^s$ represents the minimum possible Doppler frequency of the sth satellite signal at the receiver, Δf is the Doppler frequency search step size, and $F = 0, 1, 2, \ldots, F_{\max}$ is the Doppler frequency index. The transformation matrix $\mathbf{\Psi}$ (of size $[2L \times 2L]$) that we propose to sparsify the sampled received signal $\mathbf{r} = \{r[0], r[1], \ldots, r[2L-1]\}^T$ ($(\cdot)^T$ denotes the transpose operation) is a parallel correlator matrix whose element at the lth row and the kth column $\psi_{l,k}$ can be expressed as

$$\psi_{l,k} = P^s\left[\lceil (k-l)T_s R_c \rceil \,(\mathrm{mod} L)\right] \quad (3)$$

where $l, k \in \{0, 1, 2, \ldots, 2L-1\}$, L is the code length of the spreading code, and $a \pmod b$ represents the (a) modulo (b) operation. Note that the transformation matrix $\mathbf{\Psi}$ is constructed using the bank of $2L$ parallel correlators and $\mathbf{\Psi}$ transforms the input signal $\mathbf{r}$ into an approximately sparse signal with a very small sparsity $S \simeq 3$ [the number of significant values in the autocorrelation function (ACF) output] in general. Based on (3), it is obvious that

$$\mathbf{y}_0 = \mathbf{\Psi}\mathbf{r} \quad (4)$$

is a typical parallel correlator output of size $[2L \times 1]$ that represents all code phases in half-chip resolution. When f_F is close enough to f_D^s and the target signal to acquire is a binary phase-shift keying (BPSK) spread spectrum signal that has rectangular waveform, the amplitude of $\mathbf{y}_0$ becomes a typical

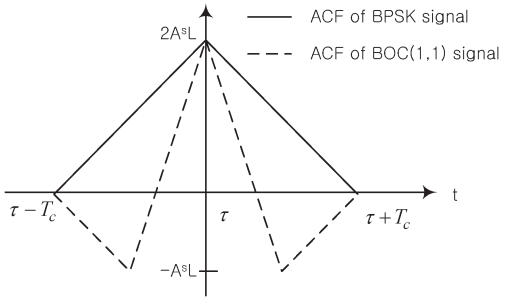

Fig. 1. ACFs: BPSK(n) and BOC(n,n).

ACF with a peak at the code phase of the incoming signal, and the elements of $\mathbf{y}_0$ can be modeled, in general, as

$$y_0[l]=\begin{cases} 2A^0\left(1-\frac{|lT_s-\tau^s|}{T_c}\right)+w^1[l]+w^2[l], & |lT_s-\tau|\le T_c \\ w^1[l]+w^2[l], & \text{otherwise} \end{cases} \tag{5}$$

where $A^0=A^sLe^{j\theta^s}$, $w^1[l]$, and $w^2[l]$ represents mutually independent complex noise generated by the correlation between the noise $n(t)$ in the sampled signal at $f_s=2R_c$ and the pseudo noise (PN) code such that

$$w^1[l]=\sum_{k=0}^{L-1}P^s\left[\left\lceil\frac{(2k-l)T_s}{T_c}\right\rceil(\mathrm{mod}L)\right]n[2kT_s] \tag{6}$$

$$w^2[l]=\sum_{k=0}^{L-1}P^s\left[\left\lceil\frac{(2k+1-l)T_s}{T_c}\right\rceil(\mathrm{mod}L)\right]n[(2k+1)T_s]. \tag{7}$$

Note that, because the triangular peak of $\mathbf{y}_0$ spans over two chips, there are at least three elements in $\mathbf{y}_0$ that contain most of the signal energy and $w^2[l]=w^1[l-1]$. For large $2L$, $w^i[l]$ ($i=1$, or 2) can be modeled by an AWGN with a probability density function (pdf) $N(0,\sigma_w^2)$, where $\sigma_w^2=LN_0$. On the other hand, when f_F is close enough to f_D^s and the target signal to acquire is a binary offset carrier (BOC) (1, 1) spread spectrum signal, the amplitude of $\mathbf{y}_0$ can generally be expressed as

$$y_0[l]=\begin{cases} 2A^0\left(1-\frac{|lT_s-\tau^s|}{T_s}\right)+w^0[l], & |lT_s-\tau|\le\frac{T_c}{2} \\ A^0\left(\frac{|lT_s-\tau^s|}{T_c}-1\right)+w^0[l], & \frac{T_c}{2}<|lT_s-\tau|\le T_c \\ (-1)^{|b-l|}w^0[l], & \text{otherwise} \end{cases} \tag{8}$$

where $w^0[l]=w^1[l]+w^2[l]$, and b is the value of l when $|lT_s-\tau^s|\le T_c/2$ is satisfied. Note that, for a receiver with a wide precorrelation bandwidth [12], the envelope of the received signal $r(t)$ (1) well maintains a rectangular shape, and as a result, the peak of the ACF output due to the signal components in $\mathbf{y}_0$ (5) and $\mathbf{y}_0$ (8) can have mean values $A^sL[1,2,1]$ and $A^sL[-1,2,-1]$, respectively, as illustrated in Fig. 1.

The proposed first-stage measurement matrix is $\mathbf{\Phi}^1$, of which an element at the mth row and the $(l+1)$th column can be defined as

$$\phi^1_{m,l+1}=\frac{(-1)^{(l+1)B}}{\sqrt{M_1}}W_{M_{01}}\left[m,\left\lceil\frac{l+1}{\alpha}\right\rceil\right] \tag{9}$$

where $1\le m\le M_1$, $0\le l\le 2L-1$, $(\cdot)^1$ denotes the first stage, $M_1=2^{M_{01}}$, $W_{M_{01}}$ is a Walsh–Hadamard matrix of size $[M_1\times M_1]$, and $\alpha(\ge 1)$ represents the number of repetition of columns of $W_{M_{01}}$. As shown in (9), $\mathbf{\Phi}^1$ has $2L$ columns made of the M_1 columns of $W_{M_{01}}$; each of the first (M_1-1) columns of $W_{M_{01}}$ is repeated α times to construct the first $\alpha(M_1-1)$ columns of $\mathbf{\Phi}^1$, and the last column of $W_{M_{01}}$ is repeated to construct the last $2L-\alpha(M_1-1)$ columns of $\mathbf{\Phi}^1$. B is a modulation scheme indicator such that $B=0$ for BPSK(n) GNSS signals and $B=1$ for BOC(n,n) GNSS signals, where n is the ratio of the signal's chip rate over the base chip rate (1.023 MHz). Other GNSS signals using BOC(b_1,b_2), where b_1 and b_2 are the subcarrier and code rates, with $b_1>b_2$, need a sampling rate higher than the $f_s(=2R_c)$ being considered in this paper. The first-stage measurement

$$\begin{aligned}\mathbf{y}_1&=\mathbf{\Phi}^1\mathbf{y}_0\\&=\mathbf{\Phi}^1\mathbf{\Psi}\mathbf{r}\end{aligned} \tag{10}$$

has a size of $[M_1\times 1]$. Notice that the first stage can be implemented with M_1 compressed correlators, which are the rows of the first-stage combined matrix $\mathbf{\Phi}^1\mathbf{\Psi}$. Therefore, the proposed technique requires about $\alpha\simeq(2L/M_1)$ times fewer measurements (i.e., correlators) in the first stage than the conventional parallel-correlator-based technique. The first line of (10) shows the first-stage measurement algorithm; $\mathbf{\Phi}^1$ encodes M_1 summations (each of which is the sum of α consecutive elements in $\mathbf{y}_0$) using M_1 Walsh codes. When $\alpha>3$, it is possible to accumulate all the signal energies spread around the peak of the ACF output (usually spreads over three neighboring samples), as expressed in (5) and (8). Because the Walsh code is an orthogonal code, the receiver can find the index of a Walsh code (e.g., w_1^T, $1\le w_1^T\le M_1$), among M_1 Walsh codes, that has the largest coefficient. The index w_1^T informs the location of the peak of ACF output (equivalently, the code phase of the incoming signal) with $(\alpha/2)$-chip resolution. Note that, due to the modulation scheme indicator B in (9), the first-stage measurement $\mathbf{y}_1$ for the BOC(n,n) signal has an identical shape and amplitude in the ACF output to $\mathbf{y}_1$ for the BPSK(n) signal, because B in (9) removes BOC modulation from the sampled data. Therefore, we assume that BPSK(n) and BOC(n,n) GNSS signals result in the same ACF, without loss of generality.

III. Detection Algorithm and the Second Stage

The first-stage detection algorithm employs M_1-point fast Walsh–Hadamard transform (FWHT) [13] to generate $\mathbf{z}_1$ (size $[M_1\times 1]$) from the first-stage observation $\mathbf{y}_1$: $\mathbf{y}_1\xrightarrow{\text{FWHT}}\mathbf{z}_1$. The purpose of applying FWHT is to find the Walsh code of which coefficient has the largest magnitude. Performing the M_1-point FWHT on both I- and Q-channel components of $\mathbf{y}_1$ (to generate I- and Q components of $\mathbf{z}_1$, respectively) requires $2M_1\log_2 M_1$ multiplications, and calculating the magnitude square of $\mathbf{z}_1$ to obtain $\mathbf{Z}_1$ (i.e., $\mathbf{Z}_1=|\mathbf{z}_1|^2$) requires additional $2M_1$ multiplications and $2M_1-1$ additions. Therefore, the

first stage requires a total of $2M_1(\log_2 M_1 + 1)$ multiplications. The elements of $\mathbf{Z}_1$ are compared to the first-stage detection threshold γ_1, and maximum N_p largest elements (larger than γ_1) of $\mathbf{Z}_1$ are selected. Let a list (set) of indices of the selected maximum N_p largest elements of $\mathbf{Z}_1$ be denoted by $\mathbf{w}_1$ such that $\mathbf{w}_1 \subset \{0, 1, 2, \ldots, M_1 - 1\}$ and $\|\mathbf{w}_1\|_0 \leq N_p$. Notice that the first-stage detection is successful if $w_1^T \in \mathbf{W}_1$ and each element of $\mathbf{w}_1$ indicates a possible peak location of the ACF output in units of α chips. Based on $\mathbf{w}_1$, we can find a list $\mathbf{W}_1$ of indices of $\mathbf{y}_0$ that can contribute to the peaks listed in $\mathbf{w}_1$ such that

$$\mathbf{W}_1 = \bigcup_{w_1 \in \mathbf{w}_1} \{\alpha w_1 + 1, \alpha w_1 + 2, \ldots, \min\{\alpha(w_1+1), 2L\}\}. \tag{11}$$

When $\mathbf{w}_1$ is empty, it can be concluded that the current Doppler frequency hypothesis is wrong and the first stage should begin with the next Doppler frequency index $F + 1$. Note that, because the variance of $w_1 \in \mathbf{w}_1$ becomes $(2\alpha - 1)$ times the variance of $w(\cdot)$ in (5) and (8), we can expect any deterministic CS matrix, of the same size to $\mathbf{\Phi}^1$, with PN codes for columns of the matrix to have poor detection performance with the transformation matrix $\mathbf{\Psi}$ that we use in this paper. There can be different transformation matrices, but $\mathbf{\Psi}$ that we use in this paper is a very strong sparsifying matrix for PN code signals. For example, supposing a sensing (measurement) matrix (size $[M_1 \times 2L]$) with columns made of PN codes, the normalized inner product between any two columns equals $(1/\sqrt{M_1})$ so that all $2L$ noise components in $\mathbf{y}_0$ contribute to the measurement $\mathbf{y}_1$ and, thus, $\mathbf{z}_1$ and $\mathbf{Z}_1$.

Let $M_{02} = \lceil \log_2 \|\mathbf{W}_1\|_0 \rceil$ and $v(= 1, 2, \ldots, \|\mathbf{W}_1\|_0)$ be the index of elements of $\mathbf{W}_1$ ($\|\mathbf{W}_1\|_0 \leq M_2$). The second stage of the proposed technique is to find the correct index (i.e., correct code phase in 0.5-chip resolution) of the peak of the ACF output in $\mathbf{y}_0$ by testing all $\|\mathbf{W}_1\|_0$ code phases listed in $\mathbf{W}_1$ using $\|\mathbf{W}_1\|_0$ parallel compressed correlators; the second-stage measurement matrix $\mathbf{\Phi}^2$ whose element at the mth row and the l-th column can be expressed as

$$\phi^2_{m,l} = \begin{cases} \frac{(-1)^{lB}}{\sqrt{M_2}} \mathbf{W}_{M_{02}}[m, v], & l = \mathbf{W}_1(v) \\ 0, & \text{otherwise} \end{cases} \tag{12}$$

where $(\cdot)^2$ denotes the second stage, $M_2 = 2^{M_{02}}$, $\mathbf{W}_{M_{02}}$ is a Walsh–Hadamard matrix of size $[M_2 \times M_2]$, and B is a modulation scheme indicator such that $B = 0$ for BPSK(n) GNSS signals and $B = 1$ for BOC(n, n) GNSS signals. Note that $\mathbf{\Phi}^2$ has $2L - \|\mathbf{W}_1\|_0$ all-zero columns, of which indices are not listed in $\mathbf{W}_1$, and depending on the choice of γ_1 and N_p, the size of $\mathbf{W}_1$ ($\|\mathbf{W}_1\|_0$) can be very small or zero. In addition, $M_2 < M_1$ can be assumed in general. Using $\mathbf{\Phi}^2$ (12), the second-stage measurement

$$\begin{aligned} \mathbf{y}_2 &= \mathbf{\Phi}^2 \mathbf{y}_0 \\ &= \mathbf{\Phi}^2 \mathbf{\Psi} \mathbf{r} \end{aligned} \tag{13}$$

is obtained. Notice that the second stage can be implemented with M_2 compressed correlators, which are the rows of the combined matrix $\mathbf{\Phi}^2\mathbf{\Psi}$, and $\mathbf{y}_2$ is a linear sum of weighted Walsh codes, i.e.,

$$\mathbf{y}_2 = \sum_{v=1}^{\|\mathbf{W}_1\|_0} \frac{(-1)^{\mathbf{W}_1(v)B}}{\sqrt{M_2}} \mathbf{y}_0(\mathbf{W}_1(v)) \mathbf{W}_{M_{02}}[\cdot, v] \tag{14}$$

where $\mathbf{W}_{M_{02}}[\cdot, v]$ represents the vth Walsh code in $\mathbf{W}_{M_{02}}$.

The proposed second-stage detection algorithm begins with M_2-point FWHT [13] to generate $\mathbf{z}_2$ (size $[M_2 \times 1]$) from the second-stage observation $\mathbf{y}_2 : \mathbf{y}_2 \xrightarrow{\text{FWHT}} \mathbf{z}_2$. Performing the M_2-point FWHT on both I- and Q-channel components of $\mathbf{y}_2$ requires $2M_2 \log_2 M_2$ multiplications, and calculating the magnitude square of $\mathbf{z}_2$ to obtain $\mathbf{Z}_2$ (i.e., $\mathbf{Z}_2 = |\mathbf{z}_2|^2$) requires additional $2M_2$ multiplications and $2M_2 - 1$ additions. Overall, the second stage requires a total of $2M_2(\log_2 M_2 + 1)$ multiplications. The maximum magnitude of $\mathbf{Z}_2$ is then compared to a detection threshold γ_2. Let $w_2(\in \{0, 1, 2, \ldots, M_2 - 1\})$ be the index of the largest element of $\mathbf{Z}_2$. Finally, $\mathbf{W}_1(w_2)$ is returned, as the final code-phase estimate of the incoming signal, to a verification function and, then, to a tracking function (i.e., delay lock loop) for continuous tracking of the signal. Notice that the final output $\mathbf{W}_1(w_2)$ expresses the estimated code phase in unit of 0.5 chips, which is a general resolution required for the verification and tracking functions to run. If the second stage results in no output, then the receiver should begin the first stage with the next Doppler frequency hypothesis $(F + 1)$. The overall two-stage compressed GNSS acquisition algorithm is summarized in Table I.

TABLE I
TWO-STAGE COMPRESSED GNSS ACQUISITION ALGORITHM

Input
$\mathbf{r} \in \mathbb{C}^{2L \times 1}$
Initial value
$F = 0$
Given parameters
Transformation matrix: $\mathbf{\Psi} \in \mathbb{C}^{2L \times 2L}$
1st-stage measurement matrix: $\mathbf{\Phi}^1 \in \mathbb{R}^{M_1 \times 2L}$
Thresholds: γ_1 and γ_2
Collection Capacity: N_p
1st-Stage
$\mathbf{y}_1 = \mathbf{\Phi}^1 \mathbf{\Psi} \mathbf{r} \in \mathbb{C}^{M_1 \times 1}$
$\mathbf{Z}_1 = |M_1\text{-point FWHT of } \mathbf{y}_1|^2 \in \mathbb{R}^{M_1 \times 1}$
$\mathbf{w}_1 = \arg\{\{N_p \text{ largest elements of } \mathbf{Z}_1\} \cap \{\mathbf{Z}_1 \geq \gamma_1\}\}$
$\mathbf{W}_1 = \{\alpha w_1, \ldots, \min\{\alpha(w_1+1), 2L+1\}| \text{ for all } w_1 \in \mathbf{w}_1\}$
If $\|\mathbf{w}_1\|_0 > 0$, proceed to the 2nd-stage with $\mathbf{W}_1$.
Otherwise, repeat the 1st-stage with $F = (F+1)(\text{mod}\,(F_{\max}+1))$.
2nd-Stage
$M_2 = 2^{\lceil \log_2 \|\mathbf{W}_1\|_0 \rceil}$
Generate 2nd-stage measurement matrix: $\mathbf{\Phi}^2 \in \mathbb{R}^{M_2 \times 2L}$
$\mathbf{y}_2 = \mathbf{\Phi}^2 \mathbf{\Psi} \mathbf{r} \in \mathbb{C}^{M_2 \times 1}$
$\mathbf{Z}_2 = |M_2\text{-point FWHT of } \mathbf{y}_2|^2 \in \mathbb{R}^{M_2 \times 1}$
$\mathbf{w}_2 = \{\arg\max \mathbf{Z}_2\} \cap \{\arg \mathbf{Z}_2 \geq \gamma_2\}$
If $\|\mathbf{w}_2\|_0 > 0$, return the index of $\mathbf{W}_1$ corresponds to $\mathbf{w}_2$ and f_F.
Otherwise, repeat the 1st-stage with $F = (F+1)(\text{mod}\,(F_{\max}+1))$.

In practice, an incoming GNSS signal may have fading so that the SNR of the incoming signal can rapidly change. To improve the sensitivity of a GNSS receiver, longer coherent

integration and noncoherent accumulation of $\mathbf{Z}_1$ and $\mathbf{Z}_2$ can be a usual choice. The procedure to generate an L_N-time noncoherently accumulated decision variable for the first and second stages $\mathbf{Z}_1^{L_N}$ and $\mathbf{Z}_2^{L_N}$ is identically the same as in the conventional technique as

$$\mathbf{Z}_1^{L_N} = \sum_{l_n=1}^{L_N} \mathbf{Z}_{1,l_n} \tag{15}$$

$$\mathbf{Z}_2^{L_N} = \sum_{l_n=1}^{L_N} \mathbf{Z}_{2,l_n} \tag{16}$$

where $\mathbf{Z}_{1,l_n}$ and $\mathbf{Z}_{2,l_n}$ represent $\mathbf{Z}_1$ and $\mathbf{Z}_2$ from the l_n-th coherent integration, respectively. Longer coherent integration with the proposed technique is discussed in Section V.

IV. Performance Analysis

The performance of the proposed compressed GNSS acquisition technique can be analyzed with receiver operating characteristic and mean acquisition time (MAT) [14] for a given coherent SNR of the transformed signal $\mathbf{y}_0$. The coherent SNR of $\mathbf{y}_0$ can be defined as [15]

$$\text{coherent SNR of } \mathbf{y}_0[\text{dB}] = 20\log_{10}\left(\frac{S_0}{2\sigma_w}\right) \tag{17}$$

where $S_0 = E[\max\{\mathbf{y}_0\}] = 2A^s L$. Denoting $\phi_{m_1}^1$ as the m_1-th column vector of the first-stage sensing matrix $\mathbf{\Phi}^1$, $\mathbf{z}_1(m_1)$ $(m_1 \in \{1, 2, \ldots, 2L\})$ can be expressed as

$$\begin{aligned}\mathbf{z}_1(m_1) &= \left\langle \phi_{m_1}^1, \mathbf{\Phi}^1 \mathbf{y}_0 \right\rangle \\ &= \sum_{n=\alpha(m_1-1)+1}^{K} y_0(n)\end{aligned} \tag{18}$$

where $K = \min\{\alpha m_1, 2L\}$, because $\phi_{m_1}^1 = \mathbf{W}_{M_{01}}(\cdot, \lceil (m_1/\alpha) \rceil)$. Therefore, the first-stage FWHT output for the I- and Q-channels has an average magnitude $S_1 \cos\theta$ and $S_1 \sin\theta$, respectively, where

$$S_1 = \begin{cases} 1.5S_0, & l_T(\text{mod}\alpha) = 0 \text{ or } 1 \\ 2S_0, & 1 < l_T(\text{mod}\alpha) \le \alpha - 1 \\ 0, & \text{otherwise} \end{cases} \tag{19}$$

and l_T $(1 \le l_T \le 2L)$ is the index of the maximum peak in $\mathbf{y}_0$, i.e., the true code phase of the incoming signal. The evaluation of S_1 in (19) is for the line-of-sight (LOS)-only channel; however, there can be a multipath channel, and most of the multipath in practice are short-delay paths that arrive within a half chip after the LOS path [16]. In the presence of both the LOS and short-delay paths, ACF output has a slightly different shape from the ACF output for the LOS-only channel; however, the LOS path is the dominant path; therefore, S_1 can be still approximated by (19) without loss of generality. The power delay spectrum [16] shows that the power of a short-delay path exponentially decreases as its delay increases so that an earlier arrival short-delay path is expected to be a stronger path. Therefore, when there is no LOS path but only short-delay paths, the ACF output is expected to have its peak at the code phase of the earliest arrival path (expected to be the strongest path) and to maintain the triangular shape. As a result, the aforementioned assumption is valid for multipath channels. Based on (19), the average value of S_1 for $0 \le l_T \ (\text{mod}\ \alpha) \le \alpha - 1$ can be expressed as

$$\overline{S}_1 = \frac{3}{\alpha} S_0 + \frac{2\alpha - 4}{\alpha} S_0 = \left(2 - \frac{1}{\alpha}\right) S_0 \tag{20}$$

and $\mathbf{z}_1$ has the same noise variance

$$\frac{1}{2} V_1 \simeq (2\alpha - 1) L N_0 \tag{21}$$

for both I- and Q-channels, which results from the accumulation of the $w(\cdot)$ in (5) and (8) for a maximum of α times.

Denoting $\phi_{m_2}^2$ $(m_2 \in \{1, 2, \ldots, 2L\})$ as the m_2-th column vector of the second-stage measurement matrix $\mathbf{\Phi}^2$, $\mathbf{z}_2(m_2)$ can be expressed as

$$\mathbf{z}_2(m_2) = \begin{cases} \left\langle \phi_{m_2}^2, \mathbf{\Phi}^2 \mathbf{y}_0 \right\rangle, & \text{for } m_2 \in \mathbf{W}_1 \\ 0, & \text{otherwise} \end{cases} \tag{22}$$

where $\langle \phi_{m_2}^2, \mathbf{\Phi}^2 \mathbf{y}_0 \rangle = y_0(m_2)$, because $\phi_{m_2}^2 = \mathbf{W}_{M_{02}}(\cdot, \lceil i_{m_2} \rceil)$ (i_{m_2} is the index of m_2 in $\mathbf{W}_1$). The signal component in the second-stage M_2-point FWHT output $\mathbf{z}_2$ has amplitudes $S_0 \cos\theta$ and $S_0 \sin\theta$ in the I- and Q-channels, respectively; therefore, $\mathbf{Z}_2$ has an average signal amplitude $S_2 = S_0$, and $\mathbf{z}_2$ has the same noise variance

$$\frac{1}{2} V_2 \simeq L N_0 \tag{23}$$

for both the I- and Q-channels.

The distribution of $Z_i \in \mathbf{Z}_i$ ($i = 1$ or 2) is a noncentral chi-square distribution with two degrees of freedom when $\mathbf{W}_1$ contains l_T, i.e.,

$$P_1^i(Z_i) = \frac{1}{V_i} \exp\left(\frac{-(Z_i + S_i^2)}{V_i}\right) I_0\left(\frac{2S_i\sqrt{Z_i}}{V_i}\right) \tag{24}$$

where $I_0(\cdot)$ is the zeroth-order modified Bessel function of the first kind or a central chi-square distribution with two degrees of freedom when $\mathbf{W}_1$ does not contain l_T, i.e.,

$$P_0^i(Z_i) = \frac{1}{V_i} \exp\left(\frac{-Z_i}{V_i}\right). \tag{25}$$

The probability of detection of the first stage can be expressed as

$$P_D^1 = \int_{\gamma_1}^{\infty} P_1^1(y) \int_0^y P_0^1(x_{(M_1 - N_s)}) dx\, dy \tag{26}$$

where $x_{(u)}$ is the uth-order statistic, and its pdf can be expressed as [17]

$$\begin{aligned} P_0^1(x_{(u)}) &= f_{x_{(u)}}(x) \\ &= \frac{M_1! \left[1 - \exp\left(\frac{-x}{V_1}\right)\right]^{u-1} \exp\left(\frac{(u - M_1 - 1)x}{V_1}\right)}{V_1 (u-1)!(M_1 - u)!}. \end{aligned} \tag{27}$$

An algebraic closed-form expression of P_D^1 (26) with the definition of $P_0^1(x_{(u)})$ (27) is not easy to find. However, the probability that the element of $\mathbf{y}_1$ carrying the signal energy is

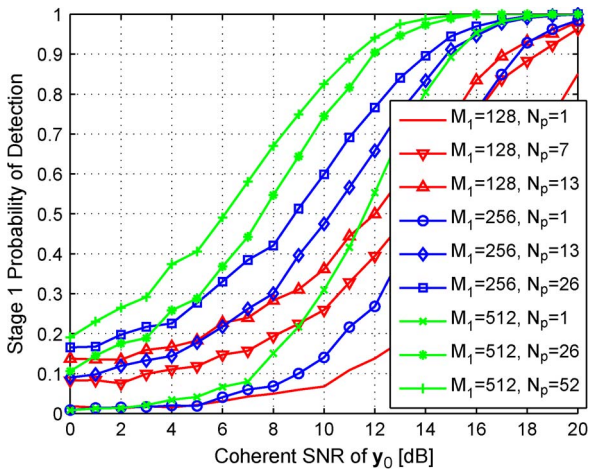

Fig. 2. First-stage probability of detection with respect to the SNR of $\mathbf{y}_0$.

included in the N_p largest elements of $\mathbf{Z}_1$ increases as N_p increases. Fig. 2 shows numerically evaluated P_D^1 (26) for various combinations of M_1 and N_p. Note that, for $N_p = 1$ and large M_1, P_D^1 (26) does not have 3-dB gain when M_1 is doubled, because $-(1/\alpha)$ in (20) is not negligible. In the following analysis, we assume $N_p = 1$ as the simplest implementation of the proposed technique and for algebraic simplicity. In general, P_D^1 (26) can be expressed by exploiting the derivations in [18] as

$$\begin{aligned} P_D^1 &\geq \int_{\gamma_1}^{\infty} P_1^1(y) \left(\int_0^y P_0^1(x)dx \right)^{M_1-1} dy \\ &\geq \sum_{n=0}^{M_1-1} \frac{(-1)^n}{n+1} \binom{M_1-1}{n} \exp\left(-\frac{nS_1^2}{(n+1)V_1} \right) \\ &\quad \times Q\left(\sqrt{\frac{2S_1^2}{(n+1)V_1}}, \sqrt{\frac{2(n+1)\gamma_1}{V_1}} \right) \end{aligned} \tag{28}$$

where the equality in (28) holds for $N_p = 1$ only, and $Q(a, b)$ is the Marcum Q-function [19]. Similarly, the probability of detection of the second stage can be expressed as

$$\begin{aligned} P_D^2 = \sum_{n=0}^{M_2-1} \frac{(-1)^n}{n+1} \binom{M_2-1}{n} \exp\left(-\frac{nS_2^2}{(n+1)V_2} \right) \\ \times Q\left(\sqrt{\frac{2S_2^2}{(n+1)V_2}}, \sqrt{\frac{2(n+1)\gamma_2}{V_2}} \right) \end{aligned} \tag{29}$$

where $M_2 = \alpha$ for $N_p = 1$. Note that, for any SNR of the incoming signal, the P_D^2 (29) is higher than the detection probability of the conventional parallel-correlator-based technique, because $M_2 \ll 2L$. In addition, using the distributions in (24) and (25) and exploiting the derivations in [18], the miss and false-alarm probabilities of the ith stage $(i = 1, 2)$ can be found, respectively, as

$$\begin{aligned} P_M^i &= \int_0^{\gamma_i} P_1^i(y)\, dy \left(\int_0^{\gamma_i} P_0^i(y)dy \right)^{M_i-1} \\ &= \left(1 - \exp\left(-\frac{\gamma_i}{V_i} \right) \right)^{M_i-1} \left[1 - Q\left(\sqrt{\frac{2S_i^2}{V_i}}, \sqrt{\frac{2\gamma_i}{V_i}} \right) \right] \end{aligned} \tag{30}$$

$$P_F^i = 1 - P_D^i - P_M^i. \tag{31}$$

Note that P_D^1 (28), P_D^2 (29), P_M^i (30), and P_F^i (31) $(i = 1, 2)$ are the probabilities when the current Doppler frequency f_F being tested is the closest Doppler frequency hypothesis to the correct Doppler frequency of the sth satellite f_D^s, i.e, $|f_F - f_D^s| < 0.5\Delta f$. Because $P_D^2 > P_D^1$, $P_M^1 \gg P_M^2$, and $P_F^1 \gg P_F^2$ for an incoming signal with good SNR and large $\alpha(\gg 1)$, P_M^2, and P_F^2 are neglected in the following analysis. When $|f_F - f_D^s| > 0.5\Delta f$, the false-alarm probability can be obtained by exploiting the derivations in [18] as

$$\begin{aligned} P_f^i &= 1 - \left(\int_0^{\gamma_i} P_0^i(y)dy \right)^{M_i} \\ &= 1 - \left[1 - \exp\left(-\frac{\gamma_i}{V_i} \right) \right]^{M_i} \end{aligned} \tag{32}$$

where $(\cdot)_f$ represents an incorrect Doppler frequency hypothesis. Notice that the probabilities P_D^1 (28), P_D^2 (29), P_M^1 (30), P_F^1 (31), and P_f^1 (32) of the proposed technique for $N_p = 1$ have the same algebraic expressions as in those of a parallel-correlator-based technique derived in [18] but with only different parameter values, i.e., reduced number of correlators M_i and SNR of the incoming signal (S_i/V_i). In a point of view, this is an expected observation, because the measurements $\mathbf{y}_1$ and $\mathbf{y}_2$ made by the proposed technique are effectively a linear combination of multiple neighboring correlator outputs (i.e., correlator outputs on neighboring code-phase hypotheses). Therefore, the performance of the proposed technique in Rayleigh fading (or AWGN) channels for an incoming signal with the SNR equal to (S_0/N_0) is the same as that of a parallel-correlator-based technique in the same Rayleigh fading (or AWGN) channels with M_i correlators for an incoming signal with the SNR equal to (S_i/V_i).

In GNSS, the N_1 of N_2 detector is one of the most widely used verification mode functions [20], and its detection and false-alarm probabilities can be found as [18]

$$\begin{aligned} P_D^V &= \sum_{n=N_1}^{N_2} \binom{N_2}{n} \left[\int_{\gamma_2}^{\infty} P_1^2(y)\, dy \right]^n \left[1 - \int_{\gamma_2}^{\infty} P_1^2(y)\, dy \right]^{N_2-n} \\ &= Q\left(\sqrt{\frac{2S_2^2}{V_2}}, \sqrt{\frac{2\gamma_2}{V_2}} \right) \end{aligned} \tag{33}$$

$$\begin{aligned} P_F^V &= \sum_{n=N_1}^{N_2} \binom{N_2}{n} \left[\int_{\gamma_2}^{\infty} P_0^2(y)\, dy \right]^n \left[1 - \int_{\gamma_2}^{\infty} P_0^2(y)\, dy \right]^{N_2-n} \\ &= \exp\left(-\frac{\gamma_2}{V_2} \right) \end{aligned} \tag{34}$$

where $(\cdot)^V$ represents the verification mode, and the correlators used in the verification mode is the same as those used in the second stage.

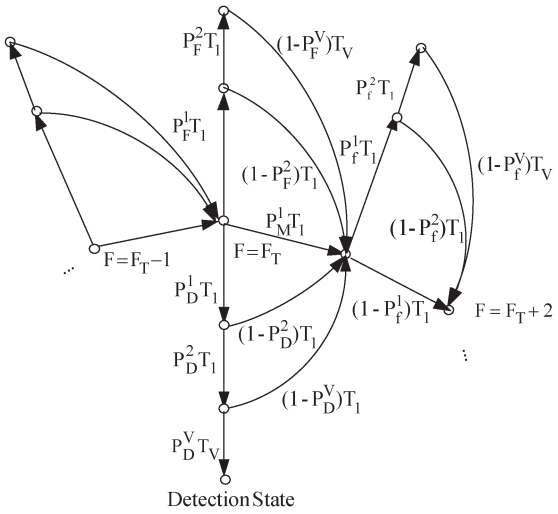

Fig. 3. Circular search state diagram.

Because the amount of time required to compute FWHT is very small, compared to the time to obtain measurements $\mathbf{y}_1$ and $\mathbf{y}_2$, we assume that both the first and second stages take $T_1 = LT_c$ s and the verification mode takes $T_V = N_2LT_c$ s. Fig. 3 shows a circular-search state-transition diagram of the proposed acquisition technique. When the current Doppler frequency hypothesis [denoted by the index F in (2)] is the closest Doppler frequency (denoted by an index F_T) to that of the incoming signal, the first-stage detection algorithm may or may not detect the signal or make a false alarm. When the first-stage algorithm misses the detection of the incoming signal, F is increased by 1 and repeats the first stage at the next node. When the first stage detects or makes a false alarm, the second-stage algorithm is invoked. The verification mode uses N_1 of N_2 detector when the second-stage algorithm declares a signal detection. The correct hypothesis detection (from node $F = F_T$ to the detection state), the correct hypothesis missed (from node $F = F_T$ to the next node $F = F_T + 1$), and the incorrect hypothesis (from node F_i to $F_{(i+1)(\bmod F_{\max})}$, $i \neq T$) branch transfer functions can be derived as

$$\begin{aligned} H_D(T) &= P_D^1 P_D^2 P_D^V T^{N_2+2} \\ &\simeq P_D^1 P_D^2 T^{N_2+2} \end{aligned} \tag{35}$$

$$\begin{aligned} H_M(T) &= P_M^1 T + P_F^1 \left(1-P_F^2\right) T^2 + P_F^1 P_F^2 \left(1-P_F^V\right) T^{N_2+2} \\ &\quad + P_D^1 \left(1-P_D^2\right) T^2 + P_D^1 P_D^2 \left(1-P_D^V\right) T^{N_2+2} \\ &\simeq P_M^1 T + P_F^1 \left(1-P_F^2\right) T^2 + P_D^1 \left(1-P_D^2\right) T^2 \\ &\quad + P_F^1 P_F^2 T^{N_2+2} \end{aligned} \tag{36}$$

$$\begin{aligned} H_0(T) &= \left(1-P_f^1\right) T + P_f^1 \left(1-P_f^2\right) T^2 \\ &\quad + P_f^1 P_f^2 \left(1-P_f^V\right) T^{N_2+1} \\ &\simeq \left(1-P_f^1\right) T + P_f^1 \left(1-P_f^2\right) T^2 + P_f^1 P_f^2 T^{N_2+1} \end{aligned} \tag{37}$$

where approximate expressions are obtained by assuming $P_D^V \simeq 1$ and $P_F^V \simeq P_f^V \simeq 0$. Note again that the miss and the false-alarm probabilities of the second stage (or in the verification mode) after a correct signal detection in the first stage (or in the second stage) are assumed negligible in (36), which is a reasonable assumption for GNSS signals of the good SNR. The overall system transfer function can be derived by exploiting the results in [14] as

$$H(T) = \frac{H_D(T)\left[1 - H_0^{F_{\max}}(T)\right]}{(F_{\max}+1)\left[1-H_0(T)\right]\left[1 - H_M(T) H_0^{F_{\max}}(T)\right]}. \tag{38}$$

Following the definition of the MAT in [14], the MAT can be obtained after some algebraic manipulations as

$$\begin{aligned} \mu_T &= T_1 \left.\frac{dH(T)}{dT}\right|_{T=1} \\ &\simeq \frac{F_{\max}T_1}{F_{\max}+1}\left[N_2 + 2 + \left(\frac{F_{\max}-1}{2}\right)\left(1+P_f^1\right)\right] \\ &\quad + \frac{F_{\max}T_1}{(F_{\max}+1)P_D^1P_D^2} \\ &\quad \times \left[1 + P_D^1 - 2P_D^1P_D^2 + P_F^1\left(1+N_2P_F^2\right)\right. \\ &\quad \left. + F_{\max}\left(1-P_D^1P_D^2\right) + N_2F_{\max}P_f^1P_f^2\right] \end{aligned} \tag{39}$$

which can further be simplified to

$$\mu_T \simeq \left[N_2 + 2 + \frac{F_{\max}}{2}\right] T_1 \tag{40}$$

for a high SNR and large $F_{\max}$, as expected. Note that, when the SNR is not high enough, the MAT μ_T increases due to the second term in (39); $P_D^1P_D^2$ in the denominator decreases, whereas the value of the numerator increases.

The detection thresholds γ_1 and γ_2 for the first and second stages, respectively, should numerically be selected to minimize the MAT, as discussed in [18]. Fig. 4 shows the MAT that was evaluated from 10^5 Monte Carlo simulations for SNR values ranging from 12 dB to 20 dB. As shown, the MAT μ_T becomes minimum when γ_1 and γ_2 are around 1.2 and 0.75, respectively, which we use for numerical evaluations of the proposed technique in Section VI.

V. Comparison With Other Techniques

The folding technique [3] and the dual-folding technique [4] have recently been introduced for faster acquisition of long PN sequences. These techniques use FFT- and IFFT-based correlations to quickly complete the acquisition procedure. By folding the receiver replica of the PN sequence multiple times, the receiver can simultaneously test multiple code-phase hypotheses, but there is an inevitable loss of the SNR due to the noise increase at the ACF output. To alleviate the SNR loss due to the folding, the dual-folding technique also employs folding of incoming signal, which requires multiple times longer reception of the incoming signal. Therefore, it may be viewed that the principle of the dual-folding technique is to use longer coherent integration of the incoming signal than the folding technique. When the receiver replica of the PN sequence and the incoming signal are folded N_f and N_i times, respectively, the folding and the dual-folding techniques can have about $10\log_{10}(1/N_f)$ dB and $10\log_{10}(N_i/N_f)$ dB SNR increase at the ACF output, respectively. Note that the SNR gain is, in fact, negative, because $N_f > N_i$ is a usual choice.

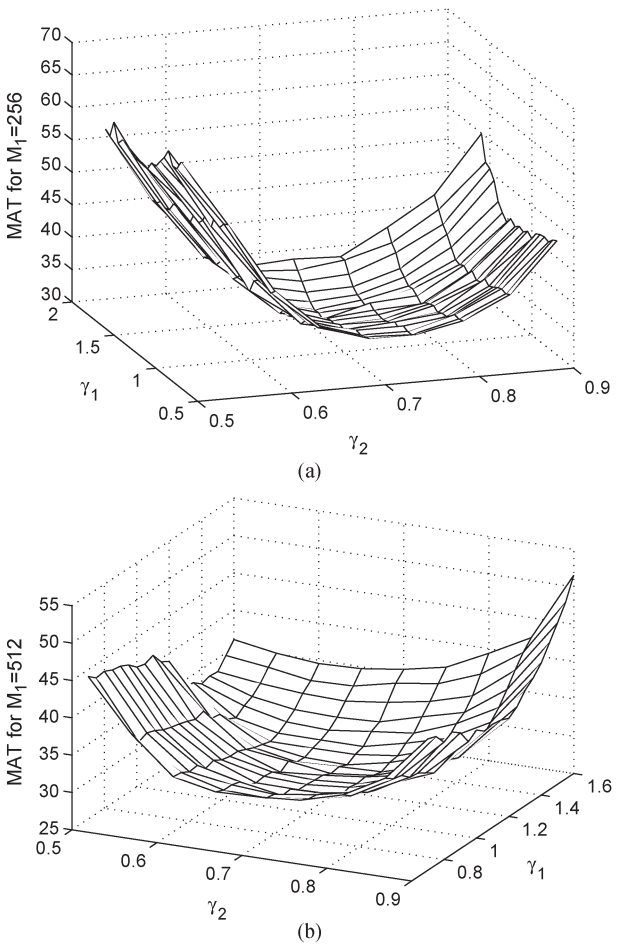

Fig. 4. MAT. (a) $M_1 = 256$. (b) $M_1 = 512$.

When the folding technique with a folding number $N_f(\gg 1)$ and the proposed technique with $\alpha = N_f$ are compared for an incoming signal samples of length $2L$, it is expected that the proposed technique should have an SNR of $(S_1)^2/(2(2N_f - 1)LN_0)$ and $(S_0)^2/(2LN_0)$ in the first- and second-stage FWHT outputs, respectively, whereas the folding technique has an SNR of $(S_0)^2/(2N_fLN_0)$ at the ACF output. Because $S_1 = (2 - 1/N_f)S_0$, the proposed technique has higher SNR gain of about $10\log_{10}(2 - 1/N_f)$ dB in the first stage, as found in (20) and (21), and $10\log_{10} N_f$ dB in the second stage than the folding technique. Therefore, for $N_f \gg 1$, the proposed technique can achieve about the same level of performance to the dual-folding technique with $N_i = 2$ and to the folding technique operating for an incoming signal with a 3-dB-high SNR.

In addition, similar to the dual-folding technique, the proposed technique can further achieve additional $10\log_{10} N_i$ dB when the size of the incoming signal samples is N_i times longer; when the length of the incoming signal samples is $2LN_i$ (i.e., N_i times longer), the transformation matrix of the proposed technique should be modified to

$$\mathbf{\Psi}_{new} = [\mathbf{\Psi}_1, \mathbf{\Psi}_2, \ldots, \mathbf{\Psi}_{N_i}] \tag{41}$$

where $\mathbf{\Psi}_k = \mathbf{\Psi}$ in (4) for all $k \in \{1, 2, \ldots, N_i\}$. Another advantage of the proposed technique is that it can simply be implemented with $M_1 + M_2$ correlators and requires $\sum_{i=1}^{2} 2M_i(\log_2 M_i + 1) \approx 2M_1(\log_2 M_1 + 1)$ complex multiplications (for large M_1 and small N_p), whereas the folding techniques require a total of $6L\log_2 2L + 2L$ complex multiplications for two FFT operations, frequency-domain multiplications, and one IFFT operation. In practice, a receiver may store an FFT PN sequence to reduce the computational complexity in the acquisition process so that the complex multiplications for the folding and the dual-folding techniques can be

$$2L(2\log_2 2L + 1). \tag{42}$$

Therefore, for an example, when $\alpha = N_f = 4$ and $L = 1023$ are assumed for $f_s = 2R_c$, the proposed technique requires at least about five times less complex multiplication than the folding and dual-folding techniques.

A deterministic CS matrix that is constructed with the second-order RM code has recently been introduced and gained attention due to the simplicity and fast reconstruction of the sparse signal from compressed measurements [10] and [11]. The CS matrix based on second-order RM codes [10] performs very well for very sparse signals; however, due to the coherence between the second-order RM codes, the performance degrades for noisy signals and less sparse signals. A deterministic CS matrix [10] of the same size as in the proposed matrix $\mathbf{\Phi}^1$ (9) can be expressed as

$$\mathbf{\Phi}_{RM} = \left[U_{P_1}, U_{P_2}, \ldots, U_{P_{\alpha-1}}, U'_{P_\alpha}\right] \tag{43}$$

where U_{P_j} is an $M_1 \times M_1$ orthogonal matrix whose columns are the second-order RM codes generated with

$$\phi_{P,b}(a) = \frac{(-1)^{wt(b)}}{\sqrt{M_1}}\sqrt{-1}^{(2b+Pa)^T a} \tag{44}$$

where P_j is a zero-diagonal symmetric binary matrix, $wt(b)$ represents the number of ones in b, b and a range through all possible binary M_{01} vectors, and U'_{P_α} is a matrix that consists of $2L - (\alpha - 1)M_1$ columns of U_{P_α}. The inner product of two arbitrary columns, each taken from different matrices U_{P_i} and U_{P_j} $(i \neq j)$, is known as

$$\left|\langle \phi_{P_i,\cdot}, \phi_{P_j,\cdot}\rangle\right| = \begin{cases} 1/\sqrt{2^l}, & 2^l \text{ times} \\ 0, & M_1 - 2^l \text{ times} \end{cases} \tag{45}$$

where $l = \text{rank}(P_i - P_j)$. In general, higher l is desirable to minimize the inner product between the columns of the matrix $\mathbf{\Phi}_{RM}$, and, thus, to minimize the amplification of noise in the ACF output. Therefore, when $l = M_{01}$, there are about $(\alpha - 1)M_1$ nonorthogonal columns in $\mathbf{\Phi}_{RM}$, which have correlation $(1/\sqrt{M_1})$ to the a column that does not belong to the $(\alpha - 1)M_1$ columns. Assuming that the same transformation matrix $\mathbf{\Psi}$ (4) is used, each column of $\mathbf{\Phi}_{RM}$ has noise components $w^1[l]$ and $w^2[l](= w^1[l+1])$ in (5). As a result, the noise variance of the measurements obtained with the sensing matrix $\mathbf{\Phi}_{RM}$ (43) can be found as

$$\begin{aligned} V_{RM} &= LN_0 \times \frac{1}{M_1} \times 4\left[(\alpha - 1)M_1 - 2\right] \\ &\simeq 4(\alpha - 1)LN_0 \end{aligned} \tag{46}$$

which is $(2\alpha - 2)/(2\alpha - 1)$ times smaller than the variance of the first-stage measurements output V_1 (21) using $\mathbf{\Phi}^1$. However, $\mathbf{\Phi}^1$ produces $(2 - 1/\alpha)^2$ times higher signal energy in the measurement output than the sensing matrix $\mathbf{\Phi}_{RM}$ (43), resulting

TABLE II
COMPARISON TO OTHER TECHNIQUES FOR $\alpha = N_f$

	Complex Multiplications	SNR of the detection variable
Proposed Technique	$\sum_{i=1}^{2} M_i \log_2(M_i+1) \approx M_1 \log_2(M_1+1)$	$10\log_{10}\frac{N_i^2(2N_f-1)S_0^2}{2N_f^2 L N_0}$ (1st-stage)
Dual Folding Technique	$4L\log_2 2L + 2L$	$10\log_{10}\frac{N_i^2 S_0^2}{2N_f L N_0}$
2nd-Order RM code	$M_1\log_2(M_1+1)$	$10\log_{10}\frac{N_i^2 S_0^2}{4(N_f-1)L N_0}$

in a net SNR gain of $10\log_{10}((2\alpha-2)(2\alpha-1)/\alpha^2)$ dB in the proposed technique. Note that the proposed first-stage sensing matrix can only estimate the code phase of the incoming signal within $(\alpha/2)$ chips; therefore, the second stage and additional collection of signal samples for $\mathbf{y}_0$ are necessary. The second-stage output has no SNR loss compared to the conventional parallel-correlator-based technique due to no increase of noise variance above $2LN_0$. On the contrary, the sensing matrix $\mathbf{\Phi}_{RM}$ (43) does not require any additional measurement. Computational complexities and the SNR gain of the proposed technique and other techniques are summarized in Table II. Note that, similar to the idea of improving the detection sensitivity of the proposed technique in (41), the measurement matrix with the second-order RM codes can exploit N_i times longer coherent integration length using a modified measurement matrix, i.e.,

$$\mathbf{\Phi}_{RM,new} = [\mathbf{\Phi}_{RM,1}, \mathbf{\Phi}_{RM,2}, \ldots, \mathbf{\Phi}_{RM,N_i}] \tag{47}$$

where $\mathbf{\Phi}_{RM,k} = \mathbf{\Phi}_{RM}$ in (43) for all $k \in \{1, 2, \ldots, N_i\}$.

In many applications of GNSS, the presence of code Doppler prevents a receiver from extending the integration length [21]. However, the transformation matrices $\mathbf{\Psi}$ (3) and $\mathbf{\Psi}_{new}$ (41) are not very suitable for a detection of signals with high code Doppler. Because each row of the transformation matrices $\mathbf{\Psi}$ and $\mathbf{\Psi}_{new}$ represents a PN-code sequence with a distinct code-phase delay at a given code rate, appropriate transformation matrices should include rows that represent the PN-code sequence with different code Doppler in addition to the rows defined in $\mathbf{\Psi}$ (3) and $\mathbf{\Psi}_{new}$ (41), which, as a result, increases the number of rows in the matrices $\mathbf{\Psi}$ and $\mathbf{\Psi}_{new}$. When, for example, three code Doppler frequencies are considered, the overall transformation matrix $\mathbf{\Psi}_{all}$ can be built as

$$\mathbf{\Psi}_{all} = \begin{bmatrix} \mathbf{\Psi}_{new,L} \\ \mathbf{\Psi}_{new,N} \\ \mathbf{\Psi}_{new,H} \end{bmatrix} \tag{48}$$

where $\mathbf{\Psi}_{new,L}$, $\mathbf{\Psi}_{new,N}$, and $\mathbf{\Psi}_{new,H}$ represent $\mathbf{\Psi}_{new}$ made with low, no, and high code Doppler frequencies, respectively. In addition, the size of the sensing matrix $\mathbf{\Phi}^i$ $(i = 1, 2)$ should accordingly be selected.

VI. NUMERICAL RESULTS

In this section, the proposed compressed GNSS acquisition technique is tested for a GPS receiver in an acquisition process of $L1$ C/A code signal, and it is assumed that the receiver has 2-MHz precorrelation bandwidth, sampling frequency $f_s = 2R_c$, and 1-ms correlation length (i.e., $2L = 2046$ samples).

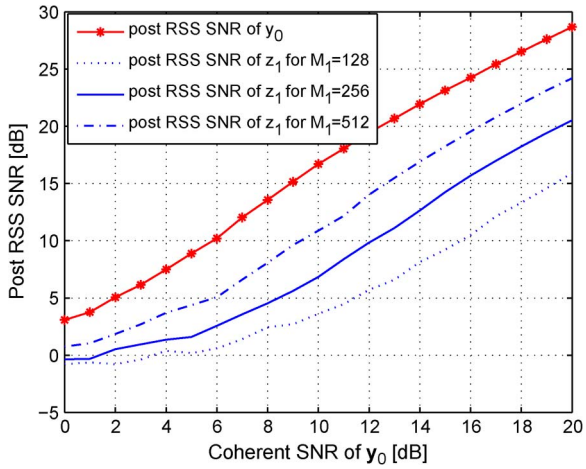

Fig. 5. Post-RSS SNR of $\mathbf{y}_1$ with respect to the SNR of $\mathbf{y}_0$.

It is obvious that the performance of the proposed technique in the acquisition of the BPSK(n) signal is the same as that in the acquisition of the BOC(n, n) signal, as discussed in Section II. The performance tests in this section show the SNR changes between the input and output signals in the first stage, the probability of detection, and MAT with respect to C/N$_0$ obtained from 10^5 Monte Carlo simulations in the AWGN channel. To compare the probability of detection of the proposed technique and the conventional parallel-correlator-based technique in various signal environments, 10^5 Monte Carlo simulations in a Rayleigh fading channel and 10^3 times field tests for ten GPS satellites are carried out. The tested C/N$_0$ ranges from 30 dB-Hz to 50 dB-Hz, which corresponds to the coherent SNR of $\mathbf{y}_0$ ranging from 0 dB to 20 dB. The parameters used in the simulations for the proposed matrices $\mathbf{\Psi}$ and $\mathbf{\Phi}$ are $M_{01} \in \{7, 8, 9\}$, $M_{02} = \log_2(2L/M_1)$, and $2L = 2046$.

Because the SNR of $\mathbf{Z}_1$ can be expressed using the post–root sum of squares (RSS) SNR of $\mathbf{z}_1$ [15], it can be found that

$$\text{post-RSS SNR of } \mathbf{z}_1 = \left(\frac{\overline{S}_1}{\sigma_{N,RSS}}\right)^2 = \text{coherent SNR of } \mathbf{y}_1 + SL \tag{49}$$

where $\sigma_{N,RSS}$ is the standard deviation of nonzero mean RSS noise, the coherent SNR of $\mathbf{y}_1$ is equal to $(\overline{S}_1^2/V_1)$, and SL is the squaring loss [15]. Fig. 5 shows the post-RSS SNR of $\mathbf{z}_1$ for $M_{01} \in \{7, 8, 9\}$ and the post-RSS SNR of $\mathbf{y}_0$ with respect to the coherent SNR of $\mathbf{y}_0$, i.e., $(S_0^2/2\sigma_w^2)$. Note that the post-RSS SNR of $\mathbf{y}_1$ for $M_{01} = 9$ is less than the post-RSS SNR of $\mathbf{y}_0$ by approximately 3 dB, as expected, based on

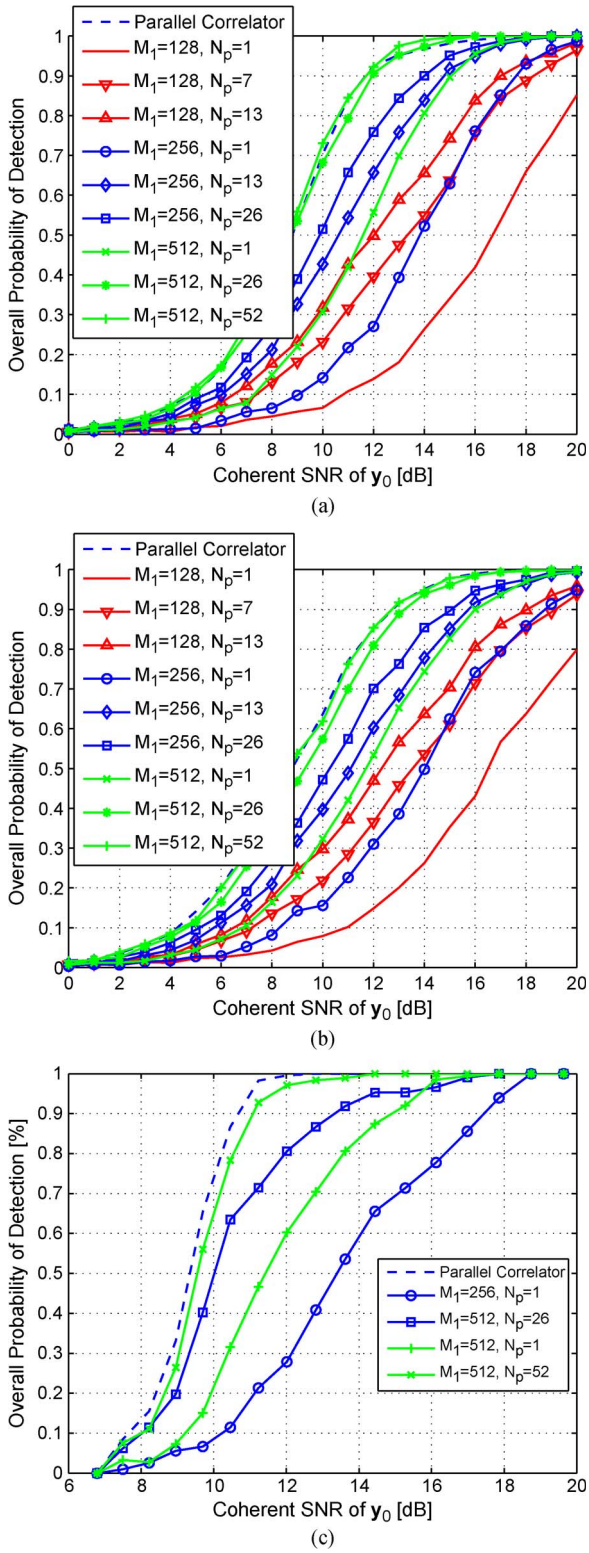

Fig. 6. Probability of detection with respect to the SNR of $\mathbf{y}_0$. (a) AWGN channel. (b) Rayleigh fading channel. (c) Real environment.

Table II, when $N_i = 1$ and $N_f = \alpha = 4$, and the post-RSS SNR of $\mathbf{y}_0$ shows positive squaring loss that is about the same as analyzed in [15]. It is obvious that the coherent SNR of the second-stage output $\mathbf{y}_2$ is the same as the coherent SNR of $\mathbf{y}_0$.

The comparison shown in Fig. 6 is between the conventional $2L$ parallel-correlator-based technique and the proposed technique with various M_1 and N_p. In the simulation, we choose $N_p = \{1, \lceil 0.05M_1 \rceil, \lceil 0.1M_1 \rceil\}$. Fig. 6(a) and (b) shows the overall probability of detection of the proposed technique and the conventional parallel-correlator-based technique with respect to the coherent SNR of $\mathbf{y}_0$ for $\gamma_1 = 1.2$ in AWGN channels and Rayleigh fading channels evaluated from 10^5 Monte Carlo simulations, respectively. Referring to the performance analysis in [4], for $f_s = R_c$, the conventional correlator-based-technique has a probability of detection about [0.4, 0.6, 0.8] at the SNR of the incoming signal about $[-20, -19, -18]$ dB, respectively. Therefore, it is expected that the same level of probability of detection can be achieved by the same technique with $f_s = 2R_c$ and about 10^3-chips-long correlation length when the coherent SNR of $\mathbf{y}_0$ is about [7, 8, 9] dB, which is roughly similar to the simulation result of the parallel correlator shown in Fig. 6(a). On the other hand, to achieve the same level of performance, the folding technique with $N_f = 4$ needs to have 3-dB higher coherent SNR of $\mathbf{y}_0$ than the proposed technique, and the dual folding technique with $N_f = 4$ needs to have $N_i = 2$ (i.e., two times longer integration). For the simulations in Rayleigh fading channel environments shown in Fig. 6(b), it is assumed that the mean power of fading channel is -7 dB, 60-km/h vehicular speed, 1-ms coherent integration length, and five times noncoherent accumulation. The results in Fig. 6(b) show that the performance is slightly worse than those in Fig. 6(a), but the relative performance of the proposed technique to that of the conventional parallel-correlator-based technique is almost the same in Fig. 6(a) and (b). Note that the proposed technique with $M_1 = 512$ and $N_p = 52$ achieves almost the same level of performance as in the parallel correlator, which means that the number of correlators to achieve the same level of acquisition performance can be about three times less than the conventional technique, because the second stage of the proposed technique requires αN_p additional correlators. The performance of the proposed technique is again compared to the conventional parallel-correlator-based technique with real GPS sampled data in Fig. 6(c), and we can again find a very similar performance to those in Fig. 6(a) and (b). Comparing the results in Fig. 6 with those in Fig. 2, it is observed that the probability of detection in the first stage P_D^1 is much higher than the overall probability of detection $P_D^1 P_D^2$ when $N_p > 1$ at a low SNR.

Fig. 7 shows the MAT μ_T (39) of the proposed technique and the conventional parallel-correlator-based technique evaluated from 10^5 Monte Carlo simulations for $M_{01} = \{7, 8, 9\}$ when $\gamma_1 = 1.2, \gamma_2 = 0.75, N_p = 4\alpha, T_1 = 1$ ms, $N_2 = 10$, and $F_{max} = 20$. The result shows that μ_T approaches the minimum average value $22T_1$ (average time to take from an arbitrary node to the node at $F = F_T$ plus times to take for the first stage, the second stage, and verification mode $= (20/2)T_1 + 2T_1 + 10T_1$) when the coherent SNR is high, as expected based on (40), and that the performance rapidly degrades for the SNR of $\mathbf{y}_0 < 12$ dB, as expected based on the second term in (39); the quantity $P_D^1 P_D^2$ in the denominator decreases, whereas the quantity $F_{max}(1 - P_D^1 P_D^2) + N_2 F_{max} P_f^1 P_f^2 + P_F^1(1 + N_2 P_F^2)$ in the numerator increases as the SNR decreases, for which a receiver needs longer coherent integration and noncoherent accumulations. Note that the MAT of the proposed technique with higher M_1 quickly approaches the

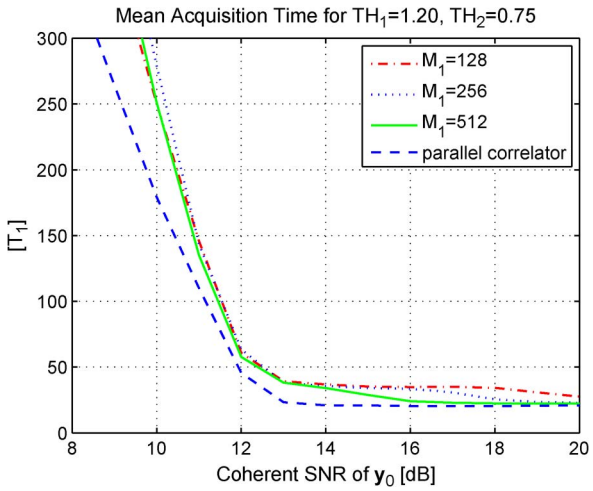

Fig. 7. MAT with respect to the SNR of $\mathbf{y}_0$.

MAT of the conventional parallel-correlator-based technique than the proposed technique with smaller M_1.

VII. Conclusion

It has been shown that the proposed compressed GNSS acquisition technique has advantages over the conventional acquisition techniques; the proposed technique requires a much lower number of correlators than the conventional parallel-correlator-based technique and much less computation than the acquisition technique using FFT/IFFT. In addition, it has been discussed that the proposed technique has better performance than the folding techniques. Because the proposed technique is a deterministic CS technique, particularly for the acquisition of spread spectrum signals, the advantage of the proposed technique is also discussed for a comparison to a deterministic CS with second-order RM codes. Note that the proposed first stage measurement scheme with small $\alpha(\leq 4)$ and $N_p(1 \ll N_p \ll M_1)$ has almost the same acquisition performance as in a conventional parallel-correlator-based technique, which is a testament to the fact that a receiver equipped with the proposed technique can have the same acquisition performance.

References

[1] B. Parkinson, J. Spilker, P. Axelrad, and P. Enge, Eds., *Global Positioning System: Theory and Applications*. Washington, DC: Amer. Inst. Aeronatics Astro., 1996.

[2] D. Akopian, "Fast FFT-based GPS satellite acquisition methods," *Proc. Inst. Elect. Eng.—Radar Sonar Navigat.*, vol. 152, no. 4, pp. 277–286, Aug. 2005.

[3] C. Yang, J. Vasquez, and J. Chaffee, "Fast direct P(Y)-code acquisition using XFAST," in *Proc. ION GPS-99*, Sep. 1999, pp. 317–324.

[4] H. Li, X. Cui, M. Lu, and Z. Feng, "Dual-folding-based rapid search method for long PN-code acquisition," *IEEE Trans. Wireless Commun.*, vol. 7, no. 12, pp. 5286–5296, Dec. 2008.

[5] E. J. Candes and T. Tao, "Decoding by linear programming," *IEEE Trans. Inf. Theory*, vol. 51, no. 12, pp. 4203–4215, Dec. 2005.

[6] D. L. Donoho, "Compressive sensing," *IEEE Trans. Inf. Theory*, vol. 52, no. 4, pp. 1289–1306, Apr. 2006.

[7] E. J. Candes and M. B. Wakin, "An introduction to compressive sampling," *IEEE Signal Process. Mag.*, vol. 25, no. 2, pp. 21–30, Mar. 2008.

[8] A. Hormati and M. Vetterli, "Annihilating filter-based decoding in the compressed sensing framework," in *Proc. Wavelets XII*, San Diego, CA, Aug. 26–30, 2007, pp. 1–10.

[9] L. Applebaum, S. Howard, S. Searle, and R. Calderbank, "Chirp sensing codes: Deterministic compressed sensing measurements for fast recovery," *Appl. Comput. Harmon. Anal.*, vol. 26, no. 2, pp. 283–290, Mar. 2009.

[10] S. D. Howard, A. R. Calderbank, and S.j. Searle, "A fast reconstruction algorithm for deterministic compressive sensing using second order Reed–Muller codes," in *Proc. CISS*, Princeton, NJ, Mar. 2008, pp. 11–15.

[11] R. Calderbank, S. Howard, and S. Jafarpour, "Construction of a large class of deterministic sensing matrices that satisfy a statistical isometry property," *IEEE J. Sel. Topics Signal Process.*, vol. 4, no. 2, pp. 358–374, Apr. 2010.

[12] P. Misra and P. Enge, *Gobal Positioning System: Signals, Measurements, and Performance,* 2nd ed. Lincoln, MA: Ganga-Jamuna, 2006.

[13] Wikipedia. [Online]. Available: http://en.wikipedia.org

[14] A. J. Viterbi, *CDMA: Principles of Spread Spectrum Communication*. Reading, MA: Addison-Wesley, 1995.

[15] F. Van Diggelen, *A-GPS: Assisted GPS, GNSS, and SBAS*. Norwood, MA: Artech House, 2009.

[16] A. Steingass and A. Lehner, "Measuring the navigation multipath channel—A statistical analysis," in *Proc. ION GNSS*, Long Beach, CA, Sep. 21–24, 2004, pp. 1157–1164.

[17] A. Papoulis, *Probabilities and Random Variables*. Englewood Cliffs, NJ: Prentice-Hall, 1990.

[18] E. A. Sourour and S. C. Gupta, "Direct-sequence spread-spectrum parallel acquisition in a fading mobile channel," *IEEE Trans. Commun.*, vol. 38, no. 7, pp. 992–998, Jul. 1990.

[19] J. I. Marcum, "A table of Q-functions," Rand Corp., Santa Monica, CA, Rep. RM-339, Jan. 1950.

[20] P. W. Ward, "GPS receiver search techniques," in *Proc. IEEE PLANS*, Atlanta, GA, Apr. 1996, pp. 604–611.

[21] I. P. Bezueha, "Mean acquisition time of serial spread spectrum PN acquisition system in the presence of Doppler code," in *Proc. IEEE 7th Int. Symp. Spread-Spectrum Tech. Appl.*, Sep. 2–5, 2002, vol. 3, pp. 751–755.

Seung-Hyun Kong (M'06) received the B.S.E.E. degree from Sogang University, Seoul, Korea, in 1992, the M.S.E.E. degree from Polytechnic University, Brooklyn, NY, in 1994, and the Ph.D. degree in aeronautics and astronautics from Stanford University, Stanford, CA, in 2006.

From 1997 to 2004, he was with Samsung Electronics Inc. and Nexpilot Inc., both in Korea, where his research focus was on Second-Generation Code-Division Multiple Access, Third-Generation Universal Mobile Telecommunication System PHY, and mobile positioning technologies. In 2006, he was with Polaris Wireless, Inc., where he was involved with hybrid positioning technology development using wireless location signature and assisted Global Navigation Satellite Systems (GNSS). From 2007 to 2009, he was a Research Staff with Qualcomm Research Center, San Diego, CA, where his R&D focus was on the indoor location technologies and advanced GNSS technologies. Since 2010, he has been an Assistant Professor with the CCS Graduate School for Green Transportation, Korea Advanced Institute of Science and Technology, Daejeon, Korea. His research interests include assisted GNSS, autonomous car navigation systems, and superresolution techniques.